Design and fabrication of wavelength tunable AWGs based on the thermo-optic effect

Pei Yuan (袁 配)[1,2], Yue Wang (王 玥)[1,*], Yuanda Wu (吴远大)[1,2], Junming An (安俊明)[1,2], and Xiongwei Hu (胡雄伟)[1]

[1]*State Key Laboratory on Integrated Optoelectronics, Institute of Semiconductors, Chinese Academy of Science, Beijing 100083, China*

[2]*College of Materials Science and Opto-Electronic Technology, University of Chinese Academy of Sciences, Beijing 100083, China*

**Corresponding authors: wy1022@semi.ac.cn*

Received September 29, 2017; accepted October 13, 2017; posted online November 9, 2017

In this Letter, a 16 channel 200 GHz wavelength tunable arrayed waveguide grating (AWG) is designed and fabricated based on the silicon on insulator platform. Considering that the performance of the AWG, such as central wavelength and crosstalk, is sensitive to the dimension variation of waveguides, the error analysis of the AWG with width fluctuations is worked out using the transfer function method. A heater is designed to realize the wavelength tunability of the AWG based on the thermo-optic effect of silicon. The measured results show that the insertion loss of the AWG is about 6 dB, and the crosstalk is 7.5 dB. The wavelength tunability of 1.1 nm is achieved at 276 mW power consumption, and more wavelength shifts will gain at larger power consumption.

OCIS codes: 060.1810, 060.4230, 230.7390, 230.7408.
doi: 10.3788/COL201816.010601.

Silicon photonics[1–3], as a low cost integration platform for datacom and telecom applications, has been drawing a lot of attention nowadays. Silicon on insulator (SOI) is an ideal material for separating passive or active devices[4–9] and their integration[10–13] because of its transparent optical property over the communication band. Besides, the mature CMOS technology can be directly applied to the integration of silicon photonics devices, which can lower their production cost greatly. With high-index contrast, the bending radius of SOI bent waveguides can be fabricated in a very small size with low loss, so the devices based on SOI may have a compact and small footprint. However, the high-index contrast of SOI material will induce some issues; for example, the properties of SOI devices are sensitive to the dimensional variation of their waveguides, thus, resulting in small fabrication tolerance and difficulty in fabrication. The arrayed waveguide grating (AWG)[14–18] is an interference device used in the wavelength division multiplexing (WDM) system, which is sensitive to the change of phase. When the regular phase is damaged, the transmission spectrum of the AWG will get worse. More concretely, when the fabrication dimension of the waveguides deviate from their designed value, the regular phase will change, then the peak wavelength of the AWG will drift, and the crosstalk will be poor as well. Therefore, compensation for the wavelength shift of the AWG is necessary. There are many reports about wavelength tunable AWGs based on silica[19], InP[20], and polymer[21], but there are only a few on wavelength tunable AWG based on SOI[22].

In this Letter, the simulation and the error analysis of AWGs with width fluctuations are worked out to analyze the influence of waveguide width on the crosstalk of the AWG. Then, the AWG with heaters for realizing channel tunability based on the thermo-optic (TO) effect of silicon is designed and fabricated.

A typical AWG consists of input/output waveguides, input/output slab waveguides, and arrayed waveguides; heaters are designed to realize the tunable wavelength, as is shown in Fig. 1. The design parameters of the 16 channel 200 GHz AWG in this Letter are listed in Table 1.

As the performance, such as peak wavelength and crosstalk of the AWG, is sensitive to the fabricated dimension, the simulation and the error analysis of AWGs with width fluctuations are worked out by adopting the transfer function method[23]. Without considering the transmission loss, the transfer function with the width fluctuations can be depicted as

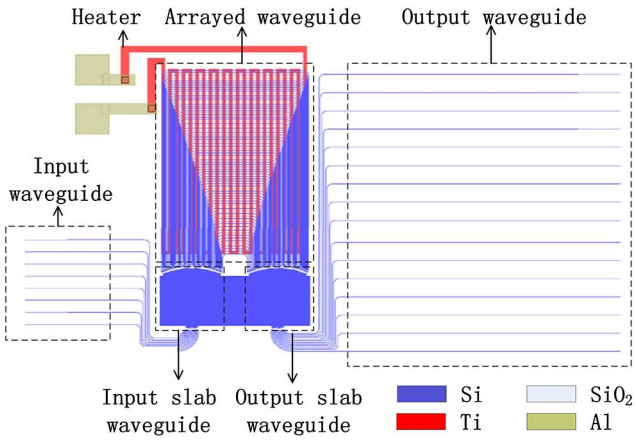

Fig. 1. (Color online) Schematic diagram of a typical AWG.

Table 1. Design Parameters of the Silicon Nanowire AWG

Parameter	Symbol	Value
Thickness of top silicon of SOI	H	220 nm
Waveguide width	w	500 nm
Thickness of slab waveguides	h	70 nm
Effective refractive index of slab waveguide	n_s	2.849257
Effective refractive index of arrayed waveguide	n_c	2.53455
Group index of arrayed waveguide	n_g	3.796747
Central wavelength	λ_0	1.55252 μm
Channel spacing	$\Delta\lambda$	1.6 nm
Number of input channels	N_i	8
Number of output channels	N_o	16
Free spectral range	FSR	25.9
Pitch width of arrayed waveguide	d	2.25
Heater spacing	D_h	10 μm
Heater width	W_h	10 μm

$$T=\left|\sum_{j=-M}^{M}[\rho_g(j,0)]^2\times\exp\left\{i\frac{2\pi}{\lambda}[j(n_{\rm cj}+{\rm rad}(n_{\rm cj}))\times\Delta L_j]\right\}\right|^2. \tag{1}$$

Here, M is the half number of arrayed waveguides, $\rho_{\rm g}(j,0)$ is the Gaussian mode field distribution of the jth arrayed waveguide, $n_{\rm cj}$ is the effective refractive index of the jth arrayed waveguide, ΔL_j is the length difference between the adjacent arrayed waveguides, and ${\rm rad}(n_{\rm cj})$ is the fluctuation of $n_{\rm cj}$ caused by the random width fluctuation (s). Random fluctuations of waveguide widths introduce random fluctuations of the refractive index of waveguides [${\rm rad}(n_{\rm cj})$], and then the transfer function (1) and the transmission spectrum of the AWG will be changed. Figure 2 shows the dependence of the effective refractive index of a waveguide on its width under different etching depths ($H_{\rm etch}$), from which it can be seen that the impact of the width fluctuation on the refractive index grows smaller with the waveguide becoming wider.

As is stated above, the random width fluctuations (s) of arrayed waveguides can impact the transmission performance of the AWG, and this influence will be reduced by using a wider waveguide. To analyze the effect of random error of the waveguide width on the transmission spectrum of the AWG, random values of arrayed waveguide widths are adopted in MATLAB using the NORMRAND command which is used to generated the random numbers that satisfy the normal distribution with mean value of 500 nm. The transmission spectra of the central channel

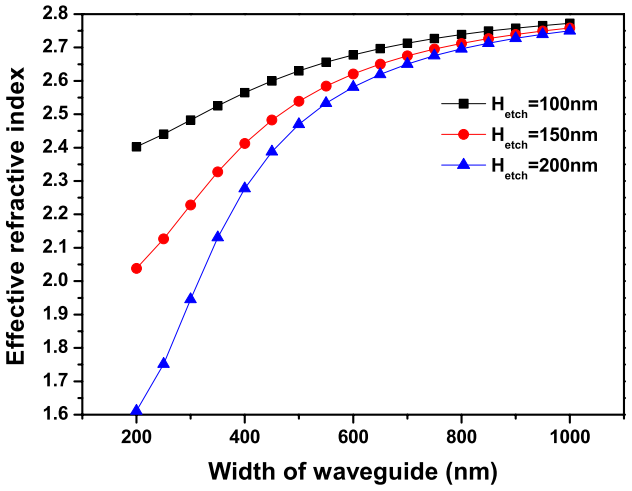

Fig. 2. (Color online) Simulated effective refractive index of the waveguide with different widths and etching depths.

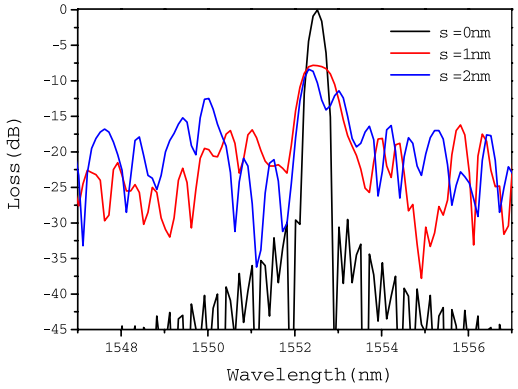

(a) Arrayed waveguide width is 500nm

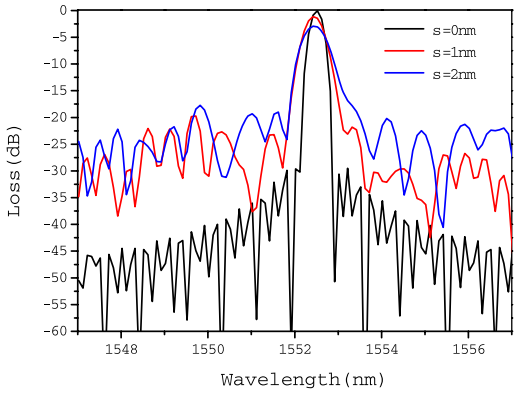

(b) Arrayed waveguide width is 800nm

Fig. 3. (Color online) Transmission spectra of the central channel of the AWG with different width fluctuations (s).

of the AWG are shown in Fig. 3(a), from which it can be seen that when the width fluctuation (s) equals 1 nm, the crosstalk will be increased to −9 dB, and when the width fluctuation is increased to 2 nm, the crosstalk will be up to about −3 dB, while the crosstalk is −30 dB with no width fluctuation.

To reduce the effect of width fluctuation on the crosstalk of the AWG, the width of the arrayed waveguides is widened to 800 nm. The transmission spectrum of the central channel is simulated with the width mean value of 800 nm, as is shown in Fig. 3(b). From Fig. 3(b), it can be seen that the crosstalk of the AWG is −21 and −15 dB, respectively, when the width fluctuation is 1 and 2 nm. In conclusion, the effect of width fluctuation on the crosstalk of the AWG can be reduced by widening the arrayed waveguides[24]. So, the waveguides in the straight section of arrayed waveguides in this Letter are widened from 500 to 800 nm, while the bend waveguides remain at 500 nm, as is shown in Fig. 4.

The simulated transmission spectrum of the AWG using the transfer function method is shown in Fig. 5, and the simulation results show that the crosstalk is less than −30 dB

To tune the peak wavelength of the AWG, a 10-μm-wide heater with a parallel structure is fabricated on the top of the AWG's arrayed waveguides, and the heater spacing is 10 μm, as is shown in Fig. 6(a). Figure 6(b) is the simulated temperature distribution when 275 mW of power consumption is applied to the heater. It can be calculated that the average temperature

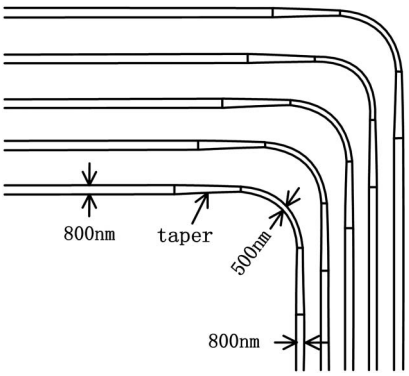

Fig. 4. Widened arrayed waveguides.

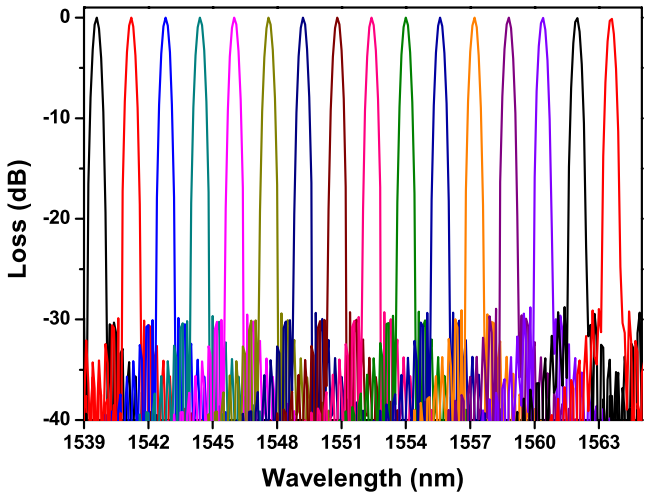

Fig. 5. (Color online) Transmission spectra of the 16 channels.

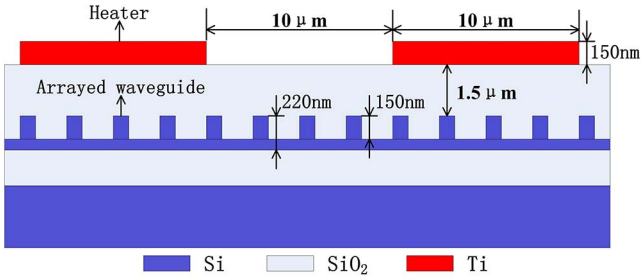

(a) The cross-section view of the arrayed waveguides and heaters

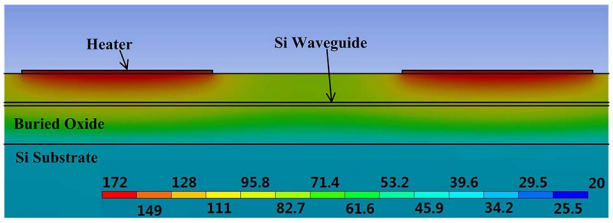

(b) The simulated temperature (°C) distribution with 275mW power consumption

Fig. 6. (Color online) Heat simulation.

of the Si waveguide layer is 35.263 °C, and the temperature of the Si waveguide is increased by 15.263 K from the room temperature of 293.15 K.

According to the TO effect, the peak wavelength shift ($\Delta\lambda$) arising from the change of temperature (ΔT) can be calculated from Eqs. (2) and (3). The TO coefficient ($\mathrm{d}n/\mathrm{d}T$) of Si equals 1.84×10^{-4}/K, and that of SiO_2 equals 1.0×10^{-5}/K:

$$\Delta n_{\mathrm{eff}} = \frac{\partial n_{\mathrm{eff}}}{\partial n_{\mathrm{Si}}} \cdot \Delta n_{\mathrm{Si}} + \frac{\partial n_{\mathrm{eff}}}{\partial n_{\mathrm{SiO_2}}} \cdot \Delta n_{\mathrm{SiO_2}}, \tag{2}$$

$$\Delta\lambda = \frac{\Delta n_{\mathrm{eff}}}{n_g} \cdot \lambda_0. \tag{3}$$

The simulated result of the relationship between the Si waveguide temperature and the applied power is shown in Fig. 7, which basically exhibits a linear function.

The wavelength tunable AWG is fabricated on the SOI chip with a 220-nm-thick top silicon layer. The thickness of the buried oxide is 2 μm. First, the mask layer for the waveguide is formed by the deep ultra-violet lithography (DUVL) process, and, then, inductively coupled plasma (ICP) etching is used to fabricate the rib waveguide. Later a 1.5-μm-thick SiO_2 layer is deposited by plasma enhanced chemical vapor deposition (PECVD). After that, titanium is deposited by the sputter and lift-off technology to form the heater. Lastly, aluminum, as the lead-wire electrode, is deposited as well.

The micrographs of the fabricated AWG are shown in Fig. 8.

The total size of the wavelength tunable AWG is 1.4 mm × 1 mm, which is quite small compared to the AWGs based on silica platform with an effective size of several centimeters squared (cm^2) and the InP platform

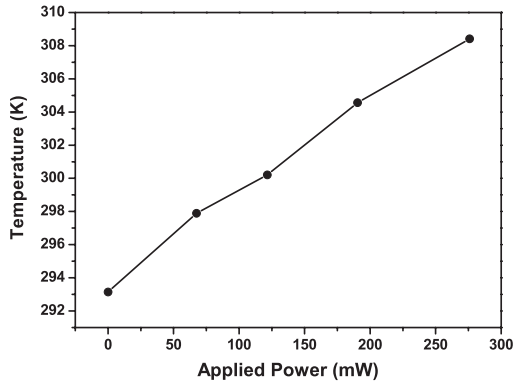

Fig. 7. Dependence of the Si waveguide's average temperature on the applied power.

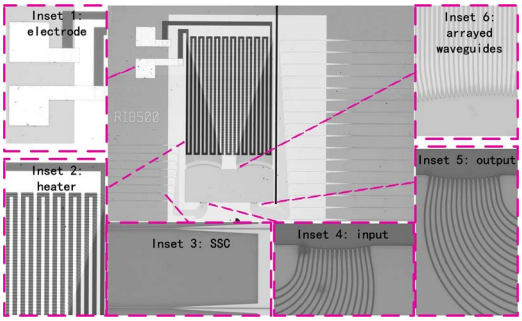

Fig. 8. Micrograph of the AWG.

with an effective size of several tens of millimeters squared (mm^2).

The measurement results of the tunable AWG are shown in Fig. 9. Figure 9 is the transmission spectra when there is no applied voltage (the solid line) and when the applied voltage is 60 V (the dotted line). From Fig. 9, it can be seen that the insertion loss of the AWG is about 6 dB, and the crosstalk is about 7.5 dB, which is very different from the simulated results. The insertion loss includes the bending loss, the loss caused by mode mismatch between two different waveguides, and the propagation loss caused by the side wall roughness. All the losses stated above are inevitable in the actual fabrication process, but not considered in the simulation.

As to the crosstalk, the high crosstalk could be the result of beam defocusing at the output waveguides due to unequal phase shifts of arrayed waveguides. As mentioned above, the refractive index of the arrayed waveguides are vulnerable to the fabrication dimension. The arrayed waveguides are widened to reduce but not to eliminate the influence of the fabrication process on the performance of the AWG. As a result, other methods must be taken to increase the tolerance of the fabrication process, such as a double etched structure at the boundary between the input/output slab waveguides and the arrayed waveguides[25]. At the same time, a fabrication process, such as ultra-violet lithography and the ICP etch process must be optimized, which is our following work.

The central wavelength of the fabricated AWG is 1563 nm, and that of the designed value is 1552.52 nm, which may be the result of waveguide width fabrication errors. As mentioned earlier, the difference between the fabricated and the designed waveguide dimensions caused by semiconductor technology, such as the DUVL process and etching technology may lead to a wavelength shift. Figure 10 shows the simulated transmission spectra of the central channel in the AWG with width deviations of 0, 5, and 10 nm, from which it can be figured out that the peak wavelength shift can reach up to 2 and 4 nm when the width deviation is 5 and 10 nm, respectively. So, it can be inferred that the width deviation can change the peak wavelength of each channel in the AWG and, therefore, greatly affect the performance of the WDM system in which the AWG is used.

Figure 11(a) is the measured transmission spectra of the 16th channel of the AWG when voltages of 0 V (0 mA), 30 V (2.25 mA), 40 V (3.04 mA), 50 V (3.81 mA), and 60 V (4.60 mA) are applied on the heating electrodes, respectively. From Fig. 11(a) it can be figured out that the tunability of the AWG is 1.077 nm at a voltage of 60 V, and the modulation efficiency of the demonstrated device is 3.902 nm/W, which performs very well among all corresponding reports. Figure 11(b) shows the simulated

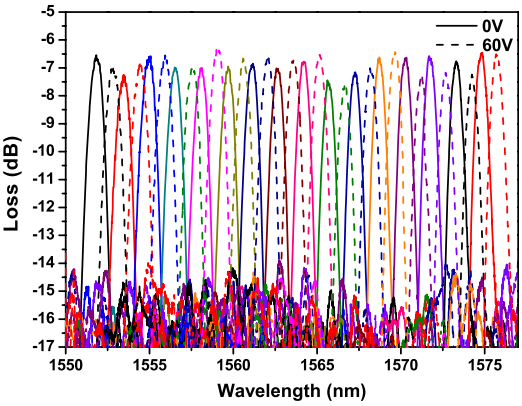

Fig. 9. (Color online) Transmission spectra with applied voltages of 0 and 60 V.

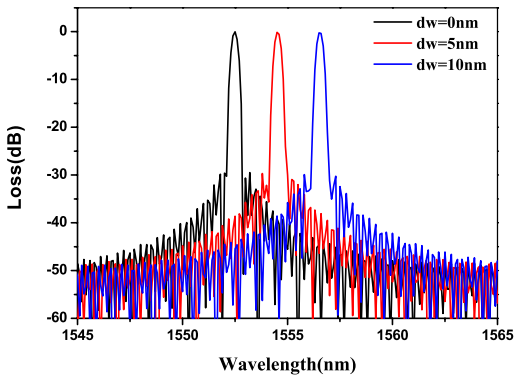

Fig. 10. (Color online) Simulated transmission spectra of the central channel of the AWG with width deviations of 0, 5, and 10 nm, respectively.

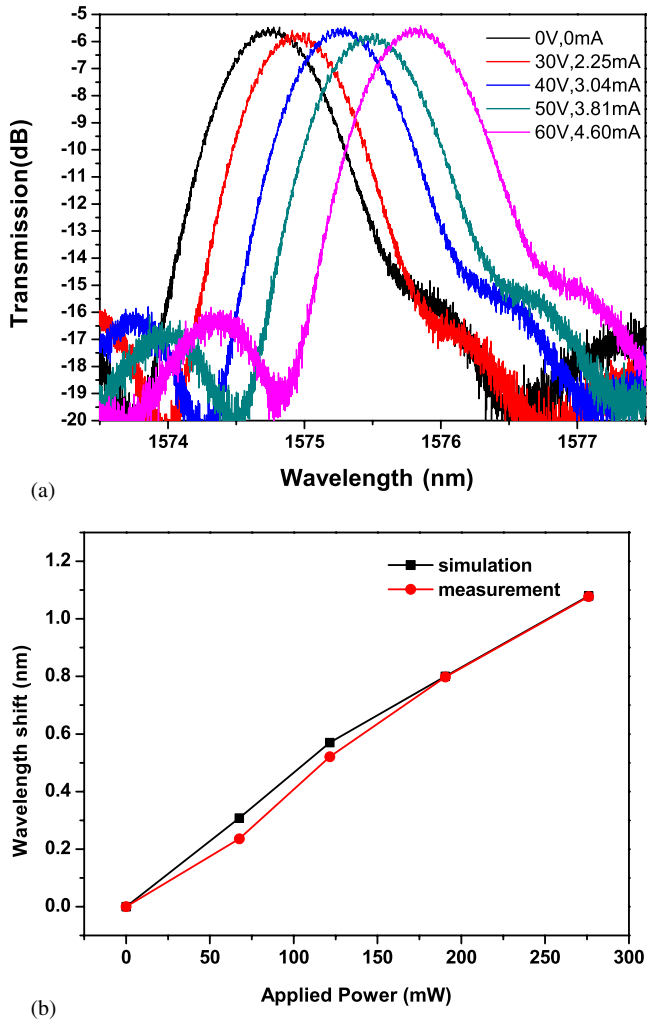

Fig. 11. (Color online) Measured wavelength compensation of the AWG under different voltages. (a) The transmission spectra of the 16th channel under different bias voltages. (b) The measured wavelength shift under different power consumptions.

and tested wavelength shifts under different power consumptions, from which it can be seen that the tested wavelength shift is in high agreement with the simulated results.

Compared with other wavelength tunable AWGs, the modulation efficiency of the AWG based on SOI performs pretty good. For example, the reported modulation efficiency of AWGs based on silica[16] is 2 nm/W. On the other hand, the modulation efficiency of the AWG in this Letter is comparable to that of the latest reported wavelength tunable AWG[19] based on SOI, whose modulation efficiency is about 3.9 nm/W, but the latter is fabricated by a more complicated processes.

In conclusion, a wavelength tunable AWG based on TO effect is demonstrated. The error analysis of the AWG with width fluctuations is worked out, and the temperature distribution of the AWG with a heater fabricated on its top is simulated, which provide the theoretical methods to improve the performances of the AWG. Besides, the wavelength tunable AWG is fabricated and tested, the results show that experiment results agree with the simulated results in terms of the TO modulation, and the modulation efficiency of the fabricated AWG can reach to 3.902 nm/W.

This work was supported by the National Key R & D Program of China (No. 2016YFB0402504) and the National Nature Science Foundation of China (Nos. 61435013 and 61405188).

References

1. M. Asghari, in *Conference on Optical Fiber Communication/National Fiber Optic Engineers Conference* (2008), paper NThA4.
2. N. B. Feilchenfeld, K. Nummy, T. Barwicz, D. Gill, E. Kiewra, R. Leidy, J. S. Orcutt, J. Rosenberg, A. D. Stricker, C. Whiting, J. Ayala, B. Cucci, D. Dang, T. Doan, M. Ghosal, M. Khater, K. Mclean, B. Porth, Z. Sowinski, C. Willets, C. Xiong, C. Yu, S. Yum, K. Giewont, and W. M. J. Green, Proc. SPIE **10149**, 101490D (2017).
3. Z. Zhou, X. Wang, H. Yi, Z. Tu, W. Tan, Q. Long, M. Yin, and Y. Huang, Opt. Eng. **52**, 5007 (2013).
4. B. Ren, Y. Hou, and Y. Liang, J. Semicond. **37**, 124001 (2016).
5. B. Song, C. Stagarescu, S. Ristic, A. Behfar, and J. Klamkin, Opt. Express **24**, 10435 (2016).
6. A. Spott, J. Peters, M. L. Davenport, E. J. Stanton, C. D. Merritt, and W. W. Bewl, Optica **3**, 545 (2016).
7. M. J. Shin, Y. Ban, B.-M. Yu, J. Rhim, L. Zimmermann, and W.-Y. Choi, IEEE J. Sel. Top. Quantum Electron. **22**, 116 (2016).
8. Z. Wang, Y. L. Gao, A. S. Kashi, J. C. Cartledge, and A. P. Knights, J. Lightwave Technol. **34**, 3675 (2016).
9. J. Lee, M. Kim, and W. Choi, Chin. Opt. Lett. **15**, 100401 (2017).
10. D. Yin, T. He, Q. Han, Q. Lv, Y. Zhang, and X. Yang, J. Semicond. **37**, 114006 (2016).
11. D. Feng, N.-N. Feng, C. C. Kung, H. Liang, W. Qian, J. Fong, B. J. Luff, and M. Asghari, Opt. Express **19**, 6125 (2011).
12. Q. Fang, J. Song, G. Zhang, M. Yu, Y. Liu, G.-Q. Lo, and D.-L. Kwong, IEEE Photon. Technol. Lett. **21**, 319 (2009).
13. P. Yuan, Y. Wu, Y. Wang, J. An, and X. Hu, J. Semicond. **36**, 084005 (2015).
14. H. Li, E. Li, Z. Liu, K. Wei, X. Dong, and Y. Bai, Opt. Eng. **51**, 123001 (2012).
15. H. Li, Y. Bai, X. Dong, E. Li, Y. Li, W. Zhou, and Y. Liu, Opt. Eng. **52**, 064602 (2013).
16. H. Li, W. Gao, E Li, and C. Tang, IEEE Photon. J. **7**, 7802707 (2015).
17. Z. Zhang, J. Hu, H. Chen, F. Li, L. Zhao, J. Gui, and Q. Fang, Chin. Opt. Lett. **15**, 041301 (2017).
18. G. Song, J. Zou, and J. He, Chin. Opt. Lett. **15**, 030603 (2017).
19. J. Dieckröger, P. C. Clemens, G. Heise, H. W. Schneider, and R. Maerz, IEEE Photon. Technol. Lett. **11**, 248 (1999).
20. H. Bissessur, F. Gaborit, B. Martin, G. Ripoche, and P. Pagnod-Rossiaux, Electron. Lett. **31**, 32 (1995).
21. H. M. Zhang, C. S. Ma, Z. K. Qin, X. Z. Zhang, D. Zhang, and D. M. Zhang, Opt. Eng. **46**, 054601 (2007).
22. Y. Yang, X. Hu, J. Song, Q. Fang, M. Yu, X. Tu, G. Q. Lo, and Rusli, IEEE Photon. Technol. Lett. **27**, 2351 (2015).
23. R. Adar, C. H. Henry, C. Dragone, R. C. Kistler, and M. A. Milbrodt, J. Lightwave Technol. **11**, 212 (1993).
24. S. Pathak, M. Vanslembrouck, P. Dumon, D. Van Thourhout, and W. Bogaerts, Opt. Express **20**, B493 (2012).
25. J. Park, J. Joo, H. Park, M. Kwack, and G. Kim, Proc. SPIE **9367**, 936705 (2015).